# A preliminary experimental study about two-sided impacting SDOF oscillator under harmonic excitation

**Ugo Andreaus, first author**[1]
Sapienza University of Rome, Faculty of Civil and Industrial Engineering, Department of Structural and Geotechnical Engineering
Via Eudossiana 18 – 00184 Rome, Italy
ugo.andreaus@uniroma1.it

**Paolo Baragatti, second author**
Sapienza University of Rome, Faculty of Civil and Industrial Engineering, Department of Structural and Geotechnical Engineering
Via Eudossiana 18 – 00184 Rome, Italy
paolo.baragatti@studiobaragatti.eu

**Maurizio De Angelis, third author**
Sapienza University of Rome, Faculty of Civil and Industrial Engineering, Department of Structural and Geotechnical Engineering
Via Eudossiana 18 – 00184 Rome, Italy
maurizio.deangelis@uniroma1.it

**Salvatore Perno, fourth author**
Sapienza University of Rome, Faculty of Civil and Industrial Engineering, Department of Structural and Geotechnical Engineering
Via Eudossiana 18 – 00184 Rome, Italy
salvatore.perno@uniroma1.it

## ABSTRACT

*Shaking table tests have been carried out to investigate the pounding phenomenon between a mass and two-sided shock absorbers, subject to sinusoidal excitations. In an effort to investigate the effectiveness of such an impact mitigation measure, preliminary tests were carried out: first, the dynamic response was recorded without pounding, and secondly the test structure was placed with gap separation and pounding was induced. Absolute acceleration, relative excursion, mean contact force, coefficient of restitution and*

[1] Corresponding author.

*dissipated energy were recorded at steady state and the excitation frequency range for pounding occurrences were determined. Numerical predictions were made by using a contact model for the simulation of impacts, able to appropriately describe the behavior of rubber under impact loading. Good agreement between the experimental and the numerical results was achieved.*

## 1 Introduction

In recent years, there has been an increasing demand to minimize structural and non-structural damage, avoid functionality disruption and protect sensitive and expensive equipments and structures even under extreme excitations. Considering that clearances exist in many civil, mechanical and industrial structures, such as heat exchangers, gear trains, bearings, nuclear power plants, etc. and that often there are practical restrictions to the width of the available gap, a reasonable concern is the possibility of poundings of systems with adjacent bodies or structures during strong excitations, i.e. it is possible that the width of the gap may not be sufficient. Therefore, it is important to investigate that possibility and understand how the maximum accelerations, displacements and contact forces of vibrating structures are affected by the various design parameters and conditions during impacts with adjacent structures.

In earthquake engineering there are some structural situations in which the clearances between adjacent structures can be limited due to practical constraints. Therefore, it is reasonable to expect that a pounding between adjacent structures occur during severe seismic excitations [1,2]. The class of block-type acceleration-sensitive equipment, whose dynamic behavior is essentially that one of rigid body, is often considered in the equipment isolation [3,4,5]; for instance, a significant portion of mechanical, electrical and electronic items is here comprised, like emergency power electric generators, Uninterruptible Power Supply (UPS) systems, transformers and computer cabinets, to mention only a few of them. In these cases, equipments can be considered as a single degree of freedom (SDOF) system [3,4,5].

Very limited experimental/numerical research studies have been conducted for impact/poundings of seismically isolated structures (beams [6,7], building, bridges, etc.).

Several research studies focused on the numerical or experimental investigation of earthquake-induced poundings of fixed-supported buildings [1,8,9]. Experimental studies [10] have shown that, in case of structural poundings, both floor accelerations and inter-story deflections are significantly amplified [11,

12]. In recent experiments, Masroor and Mosqueda [12] investigated the behavior of base isolated buildings impacting with different types of moat wall.

Shock absorbers, sometimes also known as bumpers, are mechanical devices designed to smooth out shocks and to damp vibrations [13-18]. As one of the basic mechanical components, the shock absorber has been widely used in automobiles, motorcycles, wheeled or tracked vehicles, aircrafts, as well as some industrial machines [19]. Hysteresis of structural material [10, 20-22], elastically deformable and viscously dissipative obstacles [23,24], dry friction [25,26], fluid friction [27,28] and magnetic effects [29] have been used by the absorbers for damping shock impulses.

The aim of this paper is to present a brief report which sinthetize some of the preliminary results obtained at the beginning of a series of experimental tests and numerical simulations, concerning nonlinear impact dynamics of a base-isolated SDOF oscillator excited by a harmonic base acceleration and symmetrically bounded by two unilateral deformable and dissipative constraints, say bumpers. The physical model consists of (i) a rigid body that can be treated as a lumped mass, $M$ = 500 kg (to simulate the isolated object), (ii) an elastomeric (HDRB: High Damping Rubber Bearing) isolator, the so-called damper, (iii) a couple of elastomeric bumpers. The bumpers are symmetrically mounted on steel stands which are bolted onto the base plate. The mass is comprised of six plates of mild steel jointed by through bolts. The damper is centrally connected to the lower layer of the mass; the clearance between bumpers and mass, the so-called “gap”, can be varied by adjusting the screws at the fronts of the stands; the mass is supported by four wheeled legs, rotating within unidirectional guides. The whole system is excited by the shaking table. Static tests have been first performed to determine the static characteristics and the support conditions of the shock absorbers. For readers’ convenience meaning of symbols and acronyms used throughout the paper are reported in Table 1.

## 2 Characterization of the bumper

### 2.1 Experimental set-up

The experimental investigation was preceded by a numerical investigation [30] which was used to design the experimental tests. The experiments were performed using a vibrating table Moog 1.50m×1.50m (Fig. 1). The bumper used in the experiments has width 65 mm and height 52 mm (Fig. 2) and is

constituted by an Ethylene-Propylene Diene Monomer (EPDM) having a hardness of 75 Shore A; the length of the sample is 400 mm. The mechanical characterization of the bumpers was carried out by using the machine MTS 810.

### 2.2 Cyclic tests

Experimental tests have been conducted concerning the static and dynamic behavior of the bumpers, in order to identify the mechanical characteristics useful to the numerical modeling of the whole system constituted by mass, damper and bumpers. These tests were performed subjecting the samples to programs of imposed displacement variable with sinusoidal law at different frequencies and reaching steady state after 20 cycles. The dynamic tests were carried out with a 3 mm / 200 N approach; in other words, to obtain the contact between the actuator and the sample before starting the tests, alternative initial conditions were imposed of approaching equal to 3 mm or of compressive force of 200 N.

An initial compressive displacement of about 10 mm was assigned to the specimen (compatible with the performance of the machine at the frequencies used); an excursion in displacement amplitude of about ±10 mm was subsequently imposed, in a frequency range between 0.5 Hz to 2 Hz, with a step of 0.5 Hz. The hysteresis loops shown in Fig. 3 were obtained, where also the quasi-static loop at 2 mm / min speed was reported for comparison. Limiting the comparison to the phase of initial load, dynamic stiffness appears larger than the static one. Furthermore, in the dynamical tests, cycles, around an average value of about 10 mm, are substantially superimposed, with only small differences at the extreme sides (about 2 mm and 18 mm).

In particular, it can be noted that for high values of compression load, the stiffness undergoes a significant increase, due to an important change in the form of bumper, which leads to the almost total closure of the hole and even to self-contact between the inner contours.

## 3 Results of impact tests

### 3.1 Generalities

The total gap between mass and bumpers has amplitude $\Delta = 0.03$ m. Sinusoidal accelerations with different peaks $A_t = 0.03, 0.05, 0.075, 0.1$ g(=gravity's acceleration) were imposed to the table; frequency $f$ step-wisely varied in the range $f = 0.5$ - 5.0 Hz, with step $\Delta f = 0.1$ Hz, applied for a time sufficient to reach

the steady state; the maximum values of acceleration and excursion were evaluated, of course, in correspondence of the resonance. The experimental investigations considered two distinct configurations: (a) the absence of bumper, denoted by the acronym NBs, and (b) the presence of bumper, denoted by the acronym YBs, where the system has two possible states: a situation when the mass is not in contact with the bumper, denoted *flight*, and another situation when the mass is in contact with one of the bumpers, denoted *contact*.

In both configurations, the measured parameters were the absolute acceleration of the mass and the (peak-to-peak) excursion of the relative displacement of the mass with respect to the vibrating table. The acceleration of the mass was measured by the two accelerometers positioned on the mass, in two opposite edges, as shown in Fig. 1. Maximum absolute acceleration values were recorded at steady state in each sub-frequency range of the sine sweeps, and the values averaged on the two accelerometers were taken into account. The displacement of the mass was measured by the laser transducer, as shown in Fig. 1.

The exciting action frequency was normalized with respect to the pseudo-resonance value relative to the configuration in the absence of bumpers for $A_t = 0.1g$, that is $f_R \cong 1.0$ Hz; this case corresponds to a shear deformation of the damper equal to about 100%; the normalized frequency is indicated by the symbol $\nu$. The maximum acceleration of the mass in absolute value $A_{max}$ is normalized with respect to the peak value $A_t$, and is denoted with the dimensionless parameter $\alpha = A_{max} / A_t$; the symbol $a_G = A_t / g$ will denote the non-dimensional acceleration of the shaking table. The most important results of this first experimental campaign are summarized in Table 2.

### 3.2 Configuration No-Bumpers (NBs)

Three sinusoidal accelerations with peaks $a_G = 0.03, 0.05, 0.1$ were imposed to the vibrating table. The maximum dimensionless acceleration $\alpha$ recorded at steady state of each sub-frequency range is shown in Fig. 4a. The resonance peak occurs in the neighborhood of $\nu_R = 1.2$ for $a_G = 0.03$, $\nu_R = 1.1$ for $a_G = 0.05$ and $\nu_R = 1.0$ for $a_G = 0.1$. The decrease in frequency with increasing intensity of the external action is due to softening behavior of the damper. In addition, the maximum measured dimensionless accelerations have been $\alpha = 1.80$ for $a_G = 0.03$, $\alpha = 2.99$ for $a_G = 0.05$ and $\alpha = 3.89$ for $a_G = 0.1$.

As regards the displacements, the excursion $E = (D_{max} - D_{min})$, i.e. the difference between the maximum positive displacement $D_{max}$ and the negative minimum displacement $D_{min}$, was evaluated at

steady state of each sub-frequency range; the maximum excursions (in dimensional terms) are: 0.0356 m at $a_G$ = 0.03, 0.0593 m at $a_G$ = 0.05, 0.171 m at $a_G$ = 0.1. This excursion was then normalized with respect to the maximum value of the imposed displacement, $D_{tmax} = A_t / (\Omega_{min})^2$, introducing the parameter $e = E / D_{tmax}$. The plots of the normalized excursion are shown in Fig. 4b. The maximum measured excursions are $e$ = 1.03 for $a_G$ = 0.03, $e$ = 1.715 for $a_G$ = 0.05, $e$ = 2.479 for $a_G$ = 0.1.

### 3.3 Configuration Yes-Bumpers (YBs)

Four sinusoidal accelerations with peaks $a_G$ = 0.03, 0.05, 0.075, 0.1 were imposed to the vibrating table. With regard to the relative displacements of the mass with respect to the table, the dimensionless excursion $\eta = (D_{max} - D_{min}) / \Delta$, i.e. the difference between the maximum positive displacement $D_{max}$ and minimum negative displacement $D_{min}$, normalized with respect to the total gap, was evaluated at steady state of each sub-frequency range. Having normalized the excursion with respect to the gap, a value less than 1 indicates that the mass does not touch the bumpers, the limit value 1 indicates that the mass grazes the bumpers but does not deform them, and finally $\eta > 1$ indicates that the mass has beaten and deformed the bumpers.

Figure 5a shows the maximum dimensionless acceleration in terms of the dimensionless frequency of the external excitation. Observing the figure it can be seen that, with increasing amplitude of the acceleration imposed to the table, the acceleration peak moves to the right and the acceleration value decreases: indeed resonance frequencies $\nu_R$ = 2.2, 2.5, 2.9 are observed for table accelerations $a_G$ = 0.05, 0.075, 0.1, and corresponding peak values $\alpha$ = 16.80, 16.18, 15.04. An acceleration jump is also notable, switching from high values (17-15, due to impacts) to small values (lower than one, i.e.impacts do not occur) in which the acceleration is independent of the amplitude of the action $A_t$. In the same figure the case $a_G$ = 0.03 is also reported which exhibits much smaller values of acceleration in comparison to the cases which have been previously commented. In addition, the appearance of *ridgelets* in some cases at low frequencies and of jumps from large amplitude solutions to small amplitude solutions have already been observed in numerical simulations reported in [30].

Figure 5b shows the maximum dimensionless $\eta$ excursion in terms of excitation frequency $\nu$. With reference to the three largest amplitudes of the considered excitation ($a_G$ = 0.05, 0.075, 0.1), the existence of a zone where the excursion peaks slightly grow with the action amplitude (varying from $\eta$ = 1.1 to $\eta$ =

1.3) is observable. Also the excursion, as already noticed for acceleration, exhibits a jump after which it attains a value less than one and independent of the table acceleration amplitude. In the same figure it is also shown the case $a_G = 0.03$. From the figure it is observed that only in correspondence of the resonance peak, $\nu_R = 1.3$, a value of $\eta$ slightly larger than unity is reached; therefore the collision between the mass and the bumpers occurs only at the resonance of the system.

Figures 5a and b display the envelopes of the response maxima, so as to simultaneously show the dependence of mass acceleration and displacement on amplitude $a_G$ and frequency $\nu$ of the external loading. From the above mentioned figures it can be evinced that a strong increase of acceleration occurs when the excitation amplitude grows from $a_G = 0.03$ to $a_G = 0.05$ , whereas the acceleration decreases in the further increment from $a_G = 0.075$ to $a_G = 0.1$. The value of the excursion peak, however, increases with the increase of $A_t$ and remain within the range 1.1 - 1.3, and simultaneously the frequency range $\Delta\nu_C$ widens when the impact is experienced, $\Delta\nu_C$ = 0.7-1.3, 0.7- 2.3, 0.7-3.1.

Furthermore, the possibility of obtaining a relationship between the acceleration $\alpha$ of the mass and the acceleration $a_G$ of the table appears from Fig. 5a. This relation is manifested in Fig. 6a, where it is observed a bell-shaped curve exhibiting a sort of resonance that identifies a maximum (critical) value of the peak acceleration. Representing the relation $\eta$ *vs* $a_G$ reveals that, unlike the acceleration, excursion curve is not bell-shaped but has a growing trend with $a_G$, Fig. 6b.

Considering the stationary response in correspondence with the $\nu_R$ resonance frequency in presence of bumpers, that is $\nu_R = 2.2$ for $a_G = 0.05$, $\nu_R = 2.5$ for $a_G = 0.075$, $\nu_R = 2.9$ for $a_G = 0.1$, the dimensionless force of inertia $r = F_I / (Mg)$ is diagrammed in terms of the dimensionless displacement $d = D/\Delta$ of the mass relative to the table. The first feature that is evident from Fig. 7 is constituted by the effects of mass-bumpers impact, i.e. the typical *protrusions* at the ends of the force-displacement cycles. From Fig. 7 it is observed that in the central region of the cycles ($-1 < d < +1$), when the mass is in the flight (no contact) phase, the stiffness of the system is due only to the damper, while in the two zones at the end of the cycles ($d < -1$ and $d > +1$), where the mass is in the impact phase, the stiffness of the system is due both to damper and (contacted) bumper. The cycles of Fig. 7 indicate that the stiffness of the bumper is larger than that of the damper. It is worth to be noticed, finally, that with increasing table acceleration $a_G$, a

modest increase of maximum displacement occurs with respect to a considerable increase of the maximum force.

.

### 3.4. Comparison between the two configurations YBs *vs.* NBs

The dynamic responses obtained in configurations without (NBs) and with (YBs) bumpers, are compared in this subsection. Figure 8 allows to compare, in terms of the excitation frequency ν, accelerations α (Fig. 8a) and excursions η (Fig. 8b), for three different peak values of acceleration, $a_G$ = 0.03, 0.05, 0.1.

First of all it is noted that the acceleration peak in the case YBs moves to the right compared to the case NBs and that the acceleration peak value is always higher in the case YBs with respect to that obtained in the case NBs. The peak shift to the right can be justified by the contribution in stiffness of bumpers, which adds at the impact time. It also noticed that, as $a_G$ increases, the acceleration peak is increasingly moving to the right. This is due to the fact that, with the increasing of $a_G$, also the penetration of the mass in the obstacle increases and consequently also the stiffness due to the bumpers increases, as can be seen looking at the plot of the dynamic response, measured by MTS (see Fig. 3). Also the excursion η obeys to the same trend.

Figures 8a and 8b suggest also the possibility of comparing the envelope curves of the accelerations and of the excursions in the two NBs and YBS configurations. For the acceleration, Fig. 8a, it is observed, as already said, that, in the case YBs, the peaks shift to the right (the system becomes stiffer due to the presence of the bumpers), whereas in the case NBs the peaks move to the left (for the softening behavior of the damper). In both cases the envelope curves are bell-shaped, the maximum values of which can be interpreted as critical ones. As for excursions (Fig. 8b), however, while in the case NBs the peaks move to the left and the envelope curve still has the form of a bell, in the case YBs the peaks move towards the right and the envelope curve of the maxima turns out to be a straight line with modest positive slope.

From Fig. 8 also the possibility emerges of obtaining the relationships of the acceleration α and of the excursion η in terms of the table acceleration $a_G$ for the cases YBs and NBs, Fig. 9. In this figure the resonance frequencies $\nu_R$ for the two compared situations are also indicated for each considered values of $a_G$. From Fig. 9a it is observed that the acceleration is higher in the case YBs if compared to the case NBs,

while the opposite occurs for the excursion. The quantitative comparison in terms of acceleration between the cases YBs and NBs is provided by the ratio $A_{max}$ (YBs) / $A_{max}$ (NBs); it amounts to 1.9, 5.62, 3.87 for the three considered values of $a_G$. While a considerable increase of acceleration occurs for higher values of $a_G$, differently there is only a small increase of the acceleration in the case of YBs compared to the case NBs for $a_G$ = 0.03.

The explanation may be sought in the fact that in this situation the mass grazes the bumpers and the penetration in the obstacle is so modest that only a small stiffness of the bumpers is mobilized in the first soft path of the dynamic response, see Fig. 3. The comparison in terms of excursion, Fig. 9b, between the cases YBs and NBs is quantified by the ratio $E_{max}$ (YBs) / $E_{max}$ (NBs) and is equal to 0.88, 0.62, 0.23, significantly decreasing as $a_G$ increases.

**3.5 Experimental estimation of impact parameters**

By screening the time-histories of acceleration, velocity and displacement it was possible to identify the time instants of the mass contact and detachment from bumpers in steady-state resonance conditions and the velocity values in output $v_o$ and input $v_i$, and to estimate experimentally the values of coefficients of restitution

$$s = - v_o / v_i \tag{1}$$

mean contact force in terms of the impulse momentum $I$ [31] during the contact time $\Delta t_c$

$$F_m = I / \Delta t_c \tag{2}$$

and dissipated energy $E_d$ [20]

$$E_d = ½ M (v_i)^2 - ½ M (v_o)^2 \tag{3}$$

The results of this processing are presented in Tables 3 and 4, and are also shown in the Figs. 10 and 11.

In Fig. 10a, obtained by Table 3, the mean contact force $F_m$ is shown which acts on the mass during the collision between the mass and the bumpers in terms of the table acceleration $a_G$. The mean contact force $F_m$ exhibits a trend similar to that of the dimensionless acceleration $\alpha$ (see Fig. 6a and Fig. 9a): the mean contact force has a bell-shaped form; in fact, first it has an approximately zero value of force at $a_G$ = 0.03, then a rapid increase and finally a slow decrease with increasing of $a_G$.

The contact time $\Delta t_c$, Fig. 10b, grows approximately linearly with the acceleration $a_G$. This result is justified by the fact that an increase of $a_G$ causes a deeper penetration of the mass in the bumpers.

Figure 11a, obtained by Table 4, shows the dissipated energy $E_d$ in terms of $a_G$. Energy exhibits a bell-shaped form, with a zero initial value at $a_G$ = 0.03, probably due to a negligible amount of energy dissipated by the damper and by substantially elastic impact between mass and bumper; then a peak value is attained at $a_G$ = 0.075. The value of the coefficient of restitution $s$ identified in terms of $a_G$ is shown in Fig. 11b. The coefficient is about 1 for $a_G$ = 0.03 (due to a substantially elastic behavior of the bumper) and decreases with the increase of $a_G$, attaining a minimum value $s$ = 0.75 for $a_G$ = 0.1; therefore, it remains confined in between the range $s$ = 1 - 0.75.

# 4 Physical model and equations of motion

## 4.1 Physical model

The dynamic response of the system shown in Fig. 1 is analysed as a Single-Degree-Of-Freedom (SDOF) oscillator possibly contacting double-side end stops made by means of Bumpers (Bs), Fig. 12. A mass $M$ and a non-linear isolation damper compose the SDOF oscillator. $D \equiv D_d$ denotes the relative displacement of the mass $M$ respect to the table. The rheological model of the damper, depicted in Fig. 13 and in the following text denoted by the subscript "d", is made of a tri-linear element (elastic stiffness, $K_{ed}$, yielding forces, $R_{yd1}$, $R_{yd2}$ and hardening stiffnesses, $K_{hd1}$, $K_{hd2}$) and a linear viscous damper (damping coefficient $C_d$) arranged in parallel. The piecewise-linear element, i = d, has the following constitutive law in the ($D_i \geq 0$, $R_i \geq 0$)-region:

$$R_i = K_{ei} D_i \quad 0 \leq R_i \leq R_{yi1} \quad \text{elastic phase} \tag{4a}$$

$$R_i = R_{yi1} + K_{hi1}(D_i - D_{yi1}) \quad R_{yi1} \leq R_i \leq R_{yi2} \quad 1^{st} \text{ hardening phase} \tag{4b}$$

$$R_i = R_{yi2} + K_{hi2}(D_i - D_{yi2}) \quad R_{yi2} \leq R_i \quad 2^{nd} \text{ hardening phase} \tag{4c}$$

where $D_i$, $R_i$ are the current values of displacement and force; $D_{yi1}$ and $D_{yi2}$ are the yielding displacements corresponding to $R_{yi1}$ and $R_{yi2}$, Fig. 13. Analogous laws hold in the ($D_i \leq 0$, $R_i \leq 0$)-region.

Each bumper, sketched in Fig. 12 and in the following text denoted by the subscript "b", is massless, and his rheological model is composed by a linear viscous damper (damping coefficient $C_b$) and, by a

linearly elastic element (elastic stiffness, $K_{eb}$) arranged in parallel. The relative displacement of each bumper respect to the table is denoted by $D_b$. For each bumper, the subscripts "L" and "R" are employed to respectively identify the Left and Right bumper. The element, i=b, obeys to the constitutive law of Eq. (4a).

The distance, say "gap", between the mass $M$ and the bumper is denoted by $\Delta_j(t)$, j = R, L. The system model of Fig. 12 has two bumpers located at initial distances $\Delta_{0j}$, therefore the gap function is defined as:

$$\Delta_j(t) = \Delta_{0j}(t) + \Delta D_j(t) \tag{5}$$

in which $\Delta D_R(t) = D_{bR}(t) - D_d(t)$ and $\Delta D_L(t) = D_d(t) - D_{bL}(t)$.

This system has two possible states, represented by a situation where the mass $M$ is: 1) not in contact with the bumpers, denoted *flight* ($\Delta_j(t) > 0$), and 2) in contact with at most a bumper, denoted *contact* ($\Delta_j(t) = 0$).

Moreover, it is assumed that the system is subjected to a base acceleration $A$(t) . In this paper, the ground acceleration is assumed to be harmonic, $A(t)=A_t \mathrm{Sin}\Omega t$, characterized by amplitude $A_t$ and circular frequency $\Omega = 2\,\pi\, f$.

**4.2 Equations of motion**

The equations of motion, in which ( ˙ ) denoted derivative with respect to time, are expressed in terms of the relative displacement $D_d$ and $D_b$. For the system sketched in Fig. 12, when the mass $M$ is oscillating, three situations exist and they can be described as follows:

1) the mass is not in contact with any of the bumpers

$$\begin{cases} M\ddot{D}_d + C_d\dot{D}_d + R_d = -MA_t sin(\Omega t) \\ C_{bj}\dot{D}_{bj} + R_{bj} = 0 \end{cases} \tag{6a}$$

with $\Delta_j(t) > 0$, j=R, L.

2) the mass is in contact with the Right Bumper (RB)

$$\begin{cases} M\ddot{D}_d + C_d\dot{D}_d + R_d + C_{bR}\dot{D}_{bR} + R_{bR} = -MA_t sin(\Omega t) \\ C_{bL}\dot{D}_{bL} + R_{bL} = 0 \end{cases} \tag{6b}$$

with $\Delta_R = 0$ and $D_{bR} = D_d - \Delta_{0R}$;

3) the mass is in contact with the Left Bumper (LB)

$$\begin{cases} M\ddot{D}_{\mathrm{d}} + C_{\mathrm{d}}\dot{D}_{\mathrm{d}} + R_{\mathrm{d}} + C_{\mathrm{bL}}\dot{D}_{\mathrm{bL}} + R_{\mathrm{bL}} = -MA_{\mathrm{t}}sin(\Omega t) \\ C_{\mathrm{bR}}\dot{Q}_{\mathrm{bR}} + R_{\mathrm{bR}} = 0 \end{cases} \quad (6c)$$

with $\Delta_L = 0$ and $D_{bL} = D_d - \Delta_{0L}$.

It is important to underline that dynamic response of the bumpers is governed by Eq. $(6)_2$ and hence each bumper relaxes to its original state, if there is not contact with the mass $M$. In general, the bumpers may not be at rest at the moment that a new contact phase takes place, depending on the ratio between the relaxation time of the bumper and the time interval between two contact events; therefore, influence of free motion of the bumpers is taken into account.

## 5 Numerical simulations of impact tests

The results of the experimental tests were used to identify the parameters of stiffness, strength and damping of the numerical model (see previous Sect. 4) which is able to simulate the behavior of the two-sided constraint elementary oscillator, consisting of a mass, a damper and two bumpers, by using a general-purpose computer code (Sap2000). The predictive model was implemented via an updating method. The tuning of the model parameters were performed in order to obtain a numerical model that could actually simulate the experimental dynamics in any different dynamic conditions: (i) pre-, post- and at pseudo-resonance, and (ii) in contact and in flight. In more details, the bumpers' elastic stiffness was identified by means of the dynamic tests shown in Fig. 3, with reference to the slope of the initial branch, corresponding to the partial closure of the hole; on the other hand, the damping coefficient was given by the factory ($C_b$ = 5 Ns / m). As far as damper's characteristics are concerned, the well-known behavior of elastomeric isolators [32], which are characterized by decreasing stiffness as drift increases, was assumed and schematized by a tri-linear law Fig. 13. The stiffnesses of the three branches and the damping coefficient were identified by using the three pseudo-resonance frequencies of the acceleration curves without bumpers of Fig. 4a, corresponding to the increasing table accelerations $a_G$ = 0.03, 0.05, 0.1; the yielding forces were identified by using the maximum displacements of Fig. 4b.

Definitely, the behavior of the damper was modeled with stiffness $K_{ed1}$ = 38 kN / m between $D_d$ = 0 and $D_d = D_{yd1}$=15 mm, $K_{ed2}$ = 18 kN / m between $D_d = D_{yd1}$=15 and $D_d = D_{yd2}$=40 mm, $K_{ed3}$ = 2 kN / m for $D_d > D_{yd2}$=40 mm; the linear elastic behavior of the bumpers was modelled with a stiffness $K_{eb}$ = 1460

kN / m. Moreover, the viscous behavior of damper was satisfactorily identified by linear damping coefficients $C_d$ = 1 Ns / m.

For brevity's sake, the comparisons between numerical and experimental results are reported below only in relation to the value $a_G$ = 0.05. The comparison was made with respect to the resonance curves in terms of acceleration (Fig. 14a), and excursion (Fig. 14b), and of hysteresis in the plane inertia force-displacement (Fig. 15). The solid lines represent the experimental results and the dashed lines the numerical ones; the curves seem to indicate generally a good agreement between the experimentally found results and the solutions provided by the numerical simulations, from both a qualitative and quantitative points of view.

## 6 Discussion and conclusions

In this paper a preliminary experimental and numerical investigation is briefly presented about two-sided damping constrained oscillator, when the system is subjected to harmonic excitation at the base. The testing program was planned as follows: first, the bumpers were mechanically characterized through slow (static) tests and fast (dynamic) tests via universal MTS machine; then dynamic tests on shaking table of the entire mass-damper-bumpers system were carried out. Finally, a numerical model of the single degree of freedom system has also been proposed which is able to reproduce in a sufficiently accurate manner the results achieved with the experimental tests.

The series of experimental tests on the vibrating table have considered two different configurations: the absence of bumpers (NBs) and the presence of bumpers (YBs). In both configurations tests were carried out with the same type of excitation to the base. Different values of the table acceleration peak were applied.

Generally speaking, in YBs configuration, if there is a collision between the mass and the bumpers, it is observed an increase of $\alpha$ acceleration and a decrease of $\eta$ excursion as compared to NBs configuration. It is observed, in the case YBs (see Fig. 16), that the acceleration $\alpha$ of the mass shows, with increasing $a_G$, a bell-shaped form with a (critical) peak value, while the excursion exhibits a weakly increasing linear trend. In the case NBs, as $a_G$ grows, it is observed a reduction of the resonance frequency, due to the softening behavior of the damper, and an increase of both $\alpha$, Fig. 16a, and $\eta$, Fig. 16b. It is

observed that, when the table acceleration has the amplitude $a_G$ = 0.03 (Fig. 16), the mass grazes the bumpers causing a slight increase of the resonance frequency compared to the case NBs, without an increase of acceleration and with a small reduction of excursion. It is interesting to note that, starting from the above described limit situation, with increasing $a_G$, resonance frequencies (i) increase (to the right) when the bumpers are present (and therefore the impact occurs, red line with star indicators in Fig. 16), (ii) resonance frequencies decrease (to the left) when the bumpers are not present (and thus the collision is not possible, blue line with circle indicators in Fig. 16). It is also observed that the resonance frequency of the system without bumpers (NBs configuration, blue lines with circle indicators in Fig. 17) decreases with the increase of $a_G$ (softening behavior of the damper), while that of the system with bumpers (YBs configuration, red line with star indicators in Fig. 17) increases; in fact, the system stiffness increases for the significant contribution of the bumpers; also in the latter case it is observed that the acceleration of the mass exhibits a bell-shaped form with a (critical) peak value, Fig. 17a, while the excursion remains almost constant, Fig. 17b. The mean contact force $F_m$ which acts on the mass during the phase of impact exhibits, as $a_G$ increases, Fig. 10a, a bell-shaped form. The contact time $\Delta t_c$ linearly increases with the increase of $a_G$, Fig. 10b. The dissipated energy $E_d$ in terms of $a_G$ shows, like the acceleration $\alpha$ and the mean contact force $F_m$ acting on the mass, a bell-shaped form with a well defined peak value, Fig. 11a, even if it is reached for a higher value of $a_G$.The coefficient of restitution $s$ shows a slightly decreasing trend with increasing acceleration $a_G$, Fig. 11b.

## Acknowledgment

The research was funded by the Italian Ministry of University and Research, under the Scientific Research Program of Relevant National Interest: Year 2010– 2011, Protocol 2010MBJK5B-005, Title “Dynamics, Stability and Control of Flexible Structures.”

## References


[1] Filiatrault, A., Wagner, P., and Cherry, S., 1995, "Analytical prediction of experimental building pounding", Earthq. Engng. Struct. Dyn., 24, pp. 1131–1154.

[2] Basili, M., and De Angelis, M., 2007a, "Optimal passive control of adjacent structures interconnected with non linear hysteretic devices ", J. Sound Vib., 301(1-2), pp. 106–125.

[3] Reggio, A., and DeAngelis, M., 2013, "Optimal design of an equipment isolation systemwith nonlinear hysteretic behaviour", Earthq. Engng. Struct. Dyn., 42(13), pp. 1907–1930.

[4] Reggio, A., and De Angelis, M., 2014, "Combined primary-secondary system approach to the design of an equipment isolation system with High-Damping Rubber Bearings", J. Sound Vib. 333(9), pp. 2386-2403.

[5] Basili, M., and De Angelis, M., 2014b, "Investigation on the optimal properties of semi active control devices with continuous control for equipment isolation", Scalable Computing, 15(4), pp. 331-343.

[6] Andreaus, U., Baragatti, P., and Placidi L., 2016, "Experimental and numerical investigations of the responses of a cantilever beam possibly contacting a deformable and dissipative obstacle under harmonic excitation", Int. J. Nonlin. Mech., 80, pp. 96–106.

[7] Czolczynski, K., Okolewski, A., and Blazejczyk-Okolewska, B., 2017, "Lyapunov exponents in discrete modelling of a cantilever beam impacting on a moving base", Int. J. Nonlin. Mech., 88, pp. 74-84.

[8] Polycarpou, P.C., Komodromos, P., 2010, "Earthquake-induced poundings of a seismically isolated building with adjacent structures", Eng. Struct., 32(7), pp. 1937-1951.

[9] Chau, K.T., Wie, X.X., Guo, X., and Shen, C.Y.,2003, "Experimental and theoretical simulations of seismic poundings between two adjacent structures", Earthq. Engng. Struct. Dyn., 32(4), pp. 537–54.

[10] Polycarpou, P.C., Komodromos, P. and Polycarpou, A.C., 2013, "A nonlinear impact model for simulating the use of rubber shock absorbers for mitigating the effects of structural pounding during earthquakes", Earthq. Engng. Struct. Dyn., 42(1), pp. 81–100.

[11] Papadrakakis, M., Mouzakis, H., 1995, "Earthquake simulator testing of pounding between adjacent buildings", Earthq. Engng. Struct. Dyn., 24, pp. 811–834.

[12] Masroor, A., and Mosqueda, G., 2012, "Experimental simulation of base-isolated buildings pounding against moat wall and effects on superstructure response", Earthq. Engng. Struct. Dyn., 41(14), pp. 2093-2109.

[13] Li, C., Zhu, R., Liang, M., Yang, S., 2014, "Integration of shock absorption and energy harvesting using a hydraulic rectifier", J. Sound Vib., 333(17), pp. 3904–3916.

[14] Ebrahimi, B., Khamesee, M.B., and Golnaraghi, M.F., 2008, "Design and modeling of a magnetic shock absorber based on eddy current damping effect", J. Sound Vib., 315(4–5) pp. 875–889.

[15] Serweta, W., Okolewski, A., Blazejczyk-Okolewska, B. , Czolczynski, K., and Kapitaniak, T., 2015, "Mirror hysteresis and Lyapunov exponents of impact oscillator with symmetrical soft stops" Int. J. Mech. Sci., 101-102, pp. 89-98.

[16] Hao, Z., Cao, Q., and Wiercigroch, M., 2016, "Two-sided damping constraint control strategy for high-performance vibration isolation and end-stop impact protection, Nonlinear Dynam., 86(4), pp. 2129–2144.

[17] Czolczynski, K., Blazejczyk-Okolewska, B., and Okolewski, A., 2016, "Analytical and numerical investigations of stable periodic solutions of the impacting oscillator with a moving base", Int. J. Mech. Sci., 115-116, pp. 325-338.

[18] Blazejczyk-Okolewska, B., Czolczynski, K., and Kapitaniak, T., 2010, "Hard versus soft impacts in oscillatory systems modeling", Commun. Nonlinear Sci., 15(5), pp. 1358-1367.

[19] Ren, W., Zhang, J., Jin, G., 2009, "The virtual tuning of an automatic shock absorber", J. Mech. Eng. Sci., 223(11), pp. 2655–2662.

[20] Andreaus, U., and Casini P., 2000, "Dynamics of SDOF oscillators with hysteretic motion-limiting stop", Nonlinear Dynam., **22**, pp. 155-174.

[21] Baraldi, D., Reccia, E., Cazzani, A., and Cecchi, A., 2013, "Comparative analysis of numerical discrete and finite element models: The case of in-plane loaded periodic brickwork", Composites: Mechanics, Computations, Applications, 4(4), pp. 319-344.
[22] Chiaia, B., Kumpyak, O., Placidi, L., and Maksimov, V., 2015, "Experimental analysis and modeling of two-way reinforced concrete slabs over different kinds of yielding supports under short-term dynamic loading", Eng. Struct., 96, pp. 88-99.
[23] Andreaus, U., Chiaia, B., and Placidi, L., 2013a, "Soft-impact dynamics of deformable bodies", Continuum Mech. Therm., 25(2-4), pp. 375-398.
[24] Pepe, G. , and Carcaterra, A., 2016, "VFC - Variational Feedback Controller and its application to semi-active suspensions", Mech. Syst Signal Pr., 76-77, pp. 72-92.
[25] Andreaus, U., and Casini, P., 2001, "Forced motion of friction oscillators limited by a rigid or deformable obstacle", Mech. Struct. Mach., 29(2), pp. 177-198.
[26] Koylu, H., and Cinar, A., 2011, "The influences of worn shock absorber on ABS braking performance on rough road", Int. J. Vehicle Des., 57(1), pp. 84–101.
[27] Ferdek, U., and Luczko, J.,2012, "Modeling and analysis of a twin-tube hydraulic shock absorber", J Theor. App. Mech., 50(2), pp. 627–638.
[28] Fang, Z., Guo, X., Xu, L., and Zhang, H., "Experimental study of damping and energy regeneration characteristics of a hydraulic electromagnetic shock absorber", Advances Mech. Eng., article number 943528, pp. 1-9.
[29] Amati, N., Festini, A., and Tonoli, A., 2011, "Design of electromagnetic shock absorbers for automotive suspensions", Vehicle Syst. Dyn., 49(12), pp. 1913–1928.
[30] Andreaus, U., and De Angelis, M., 2016, "Nonlinear dynamic response of a base-excited SDOF oscillator with double-side unilateral constraints", Nonlinear Dynam., 84(3), pp. 1447–1467.34
[31] Balachandran, B., 2003, "Dynamics of an elastic structure excited by harmonic and aharmonic impactor motions", J. Vib. Control, 9(3), pp. 265–279.
[32] Naeim, F., and Kelly, J., 1999, Design of Seismic Isolated Structures: From Theory to Practice, John Wiley and Sons, NY.

**Figure captions list**

**Table captions list**

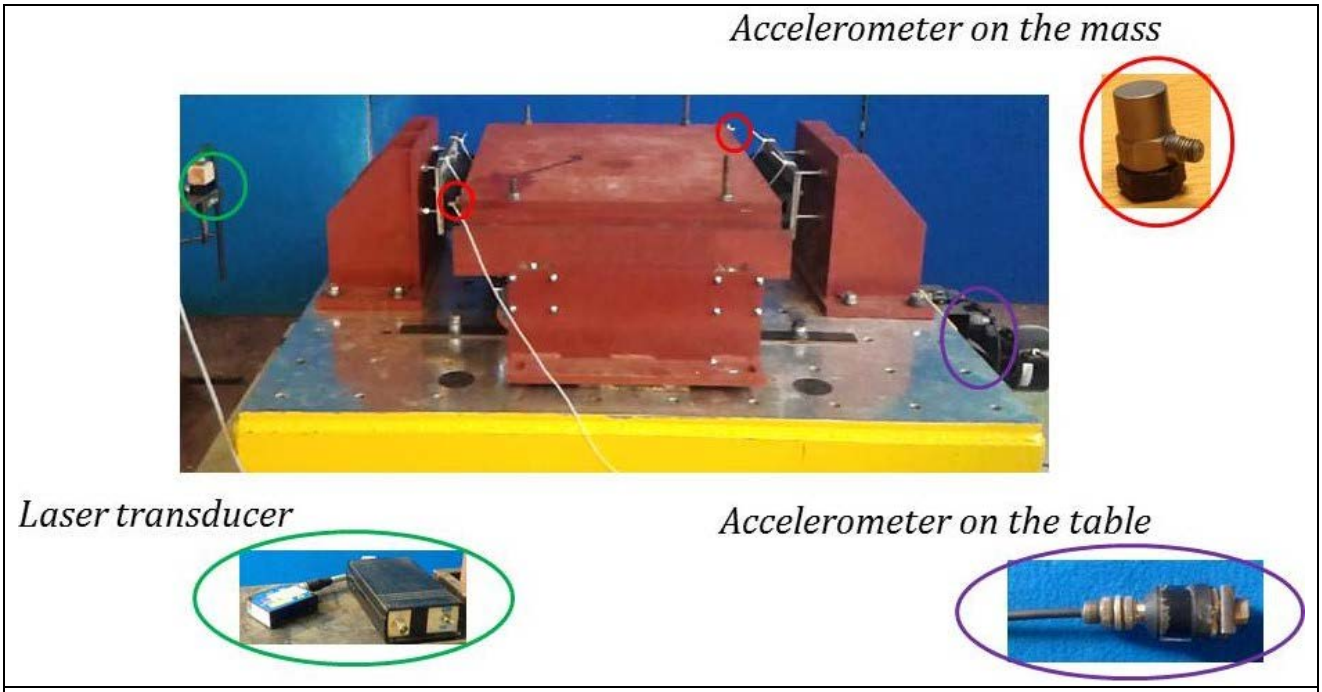


**Fig. 1** Experimental setup for impact testing

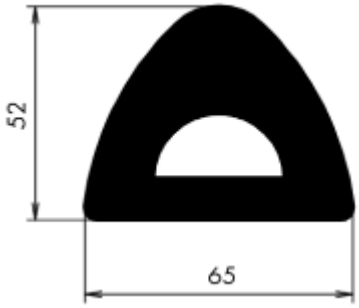


**Fig. 2** D-shaped bumper profile

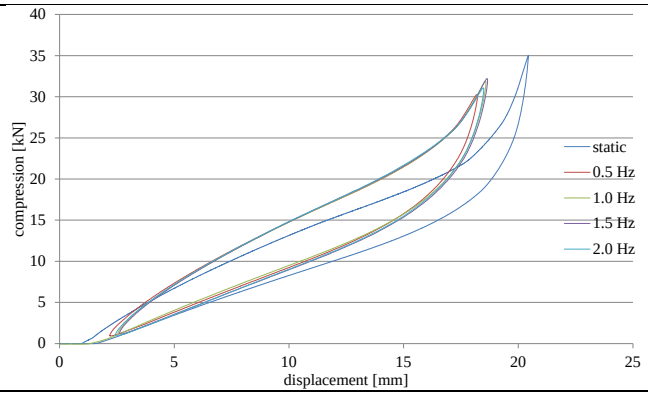


**Fig. 3** Comparison of static and dynamic tests of the bumper at various frequencies

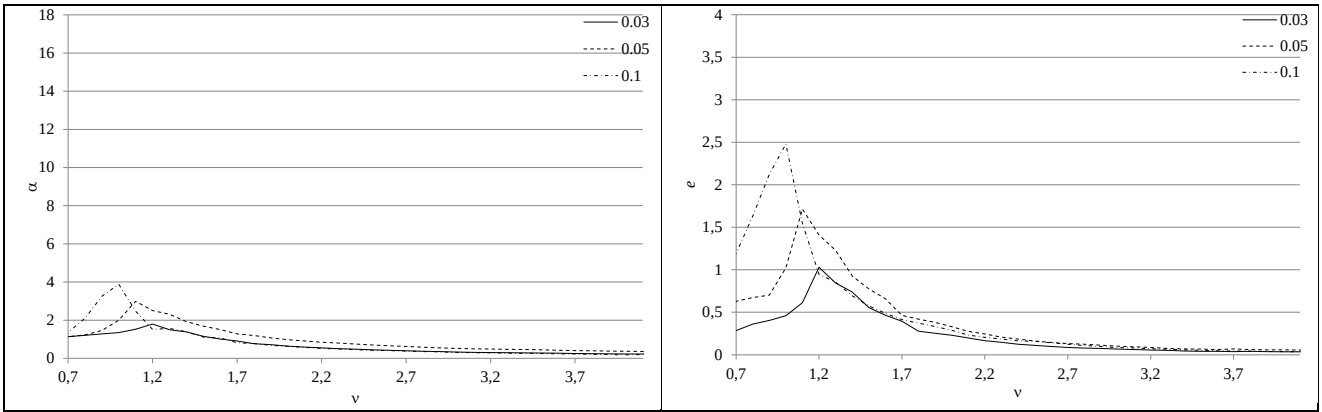


a) Acceleration

b) Excursion

**Fig. 4** NBs - Pseudo FRFs

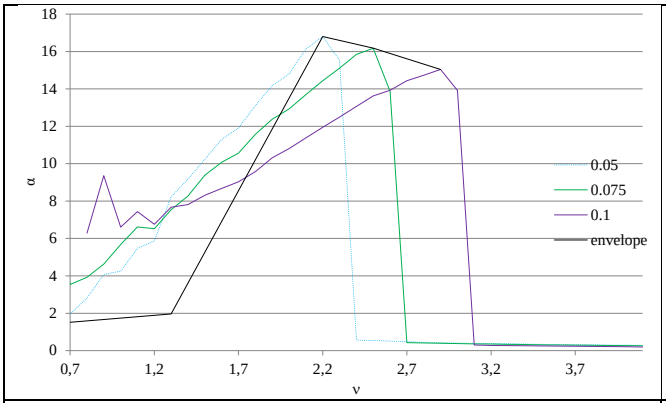


a) Acceleration

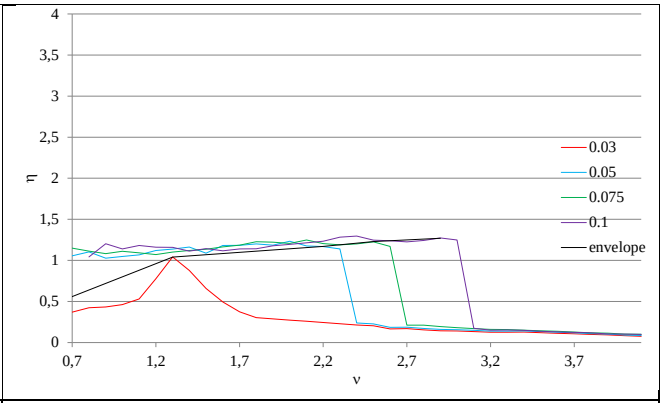


b) Excursion

**Fig. 5** YBs - Pseudo FRFs

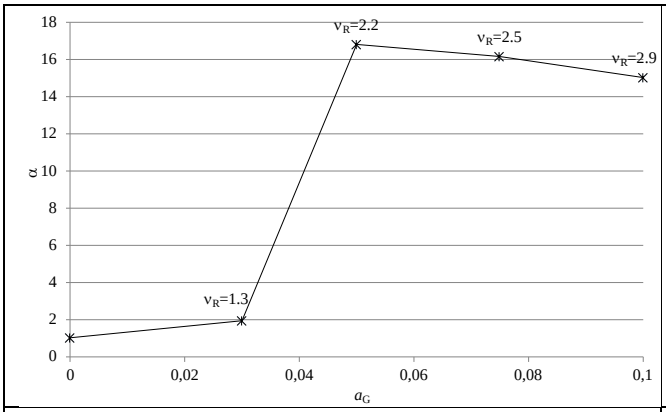


a) Acceleration

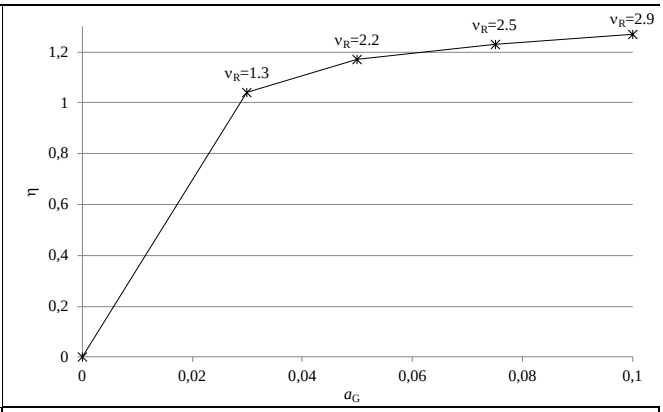


b) Excursion

**Fig. 6** YBs - α and η *vs.* $a_G$

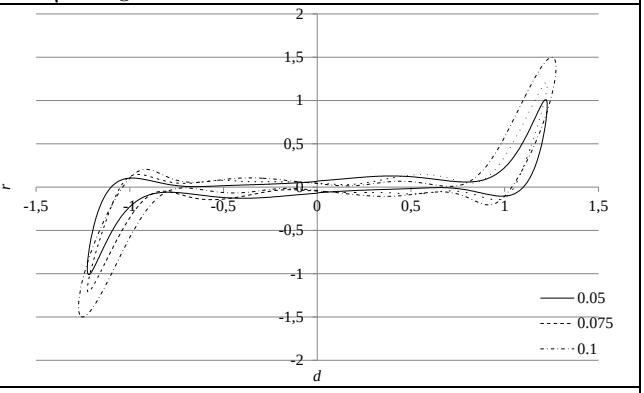


**Fig. 7** YBs - $a_G$=0.05,0.075,0.1 - Inertia force *vs.* relative displacement at resonance

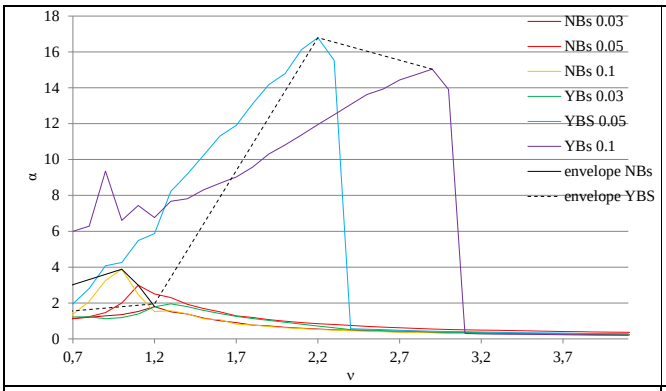


a) Acceleration

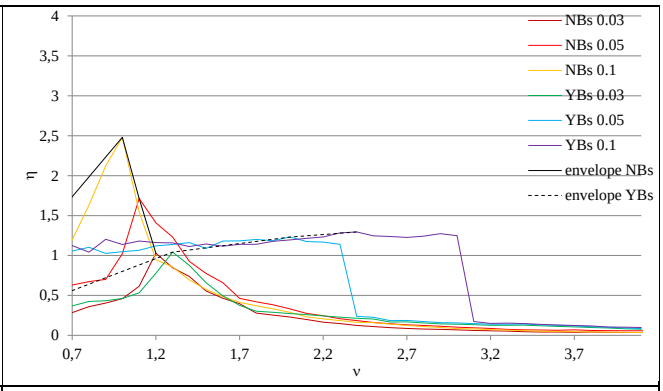


b) Excursion

**Fig. 8** YBs – Pseudo FRFs

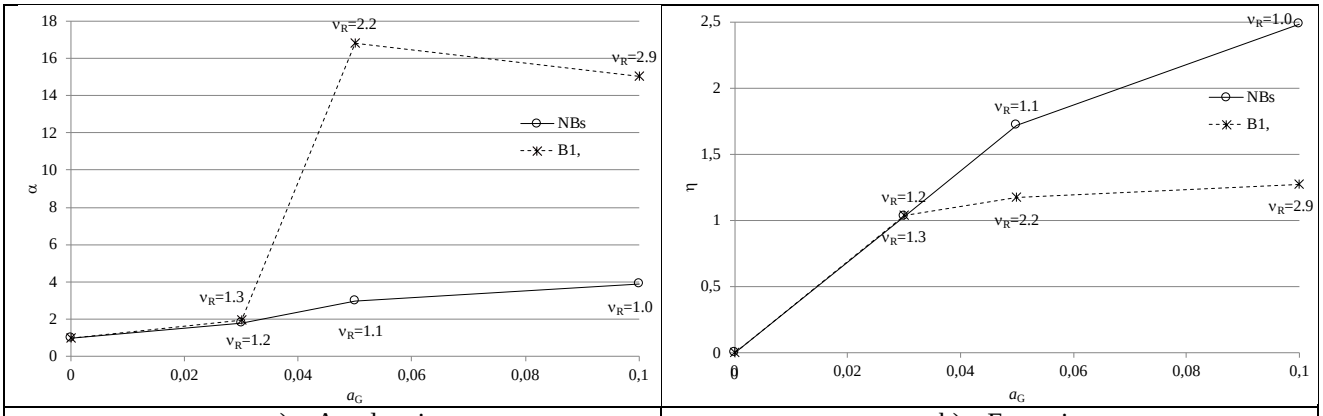


a) Acceleration b) Excursion

**Fig. 9** NBs *vs.* YBs: α and η vs. $a_G$

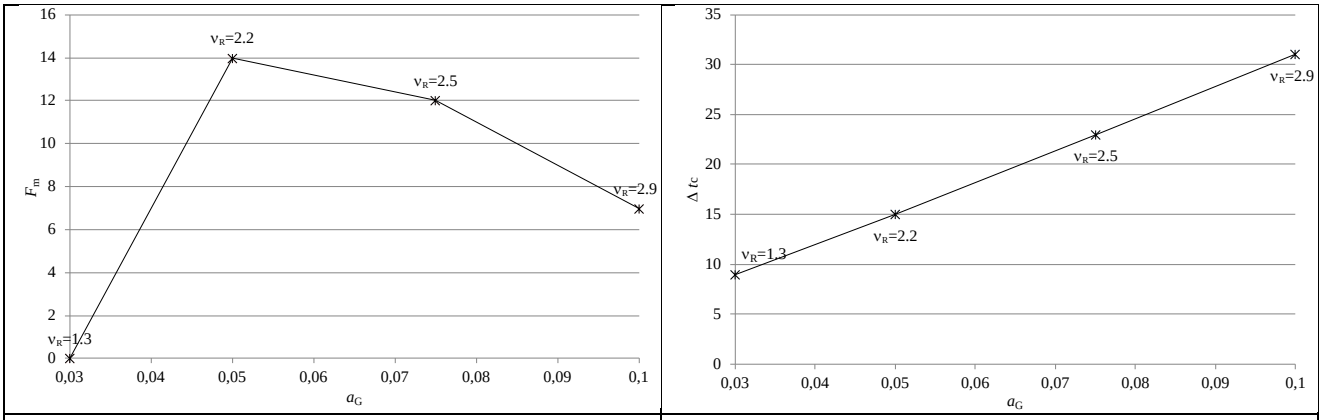


a) Mean force b) Contact time

**Fig. 10** Mean force and contact time in terms of table acceleration

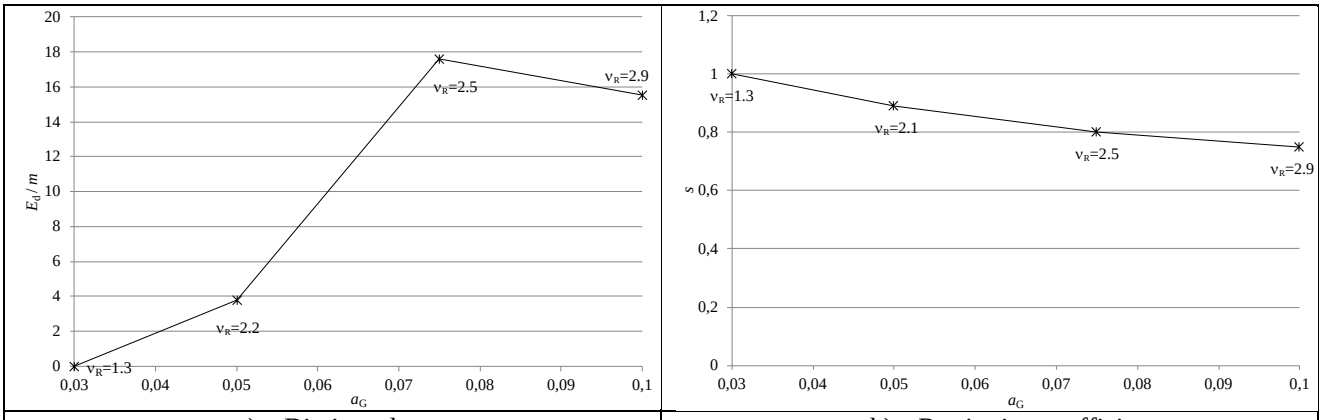


a) Dissipated energy b) Restitution coefficient

**Fig. 11** Dissipated energy and restitution coefficient in terms of table acceleration

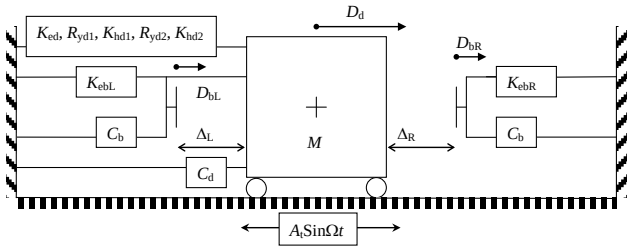


**Fig. 12** SDOF oscillator and double-side end stops

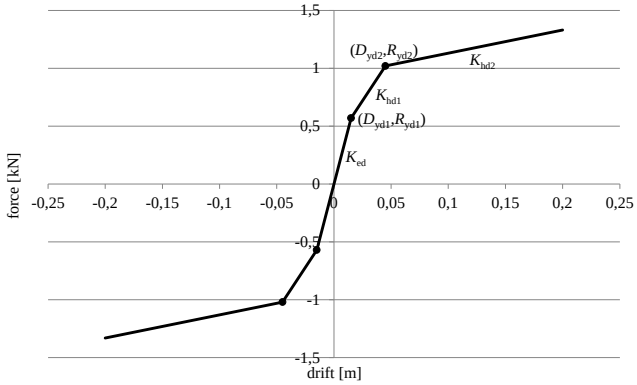


**Fig. 13** Tri-linear constitutive law of damper

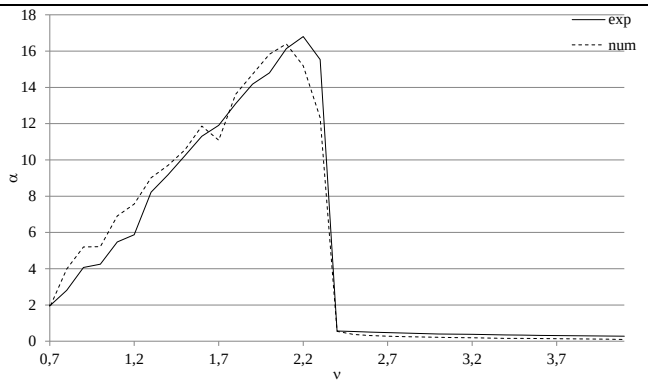


a) Acceleration

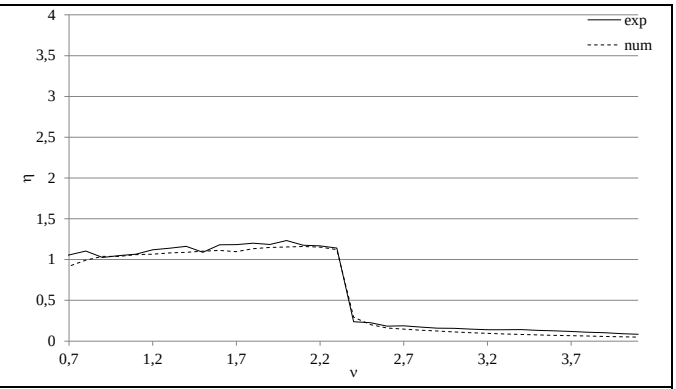


b) Excursion

**Fig. 14** YBs, $a_G$=0.05 (solid line: experimental results, dashed line: numerical results)

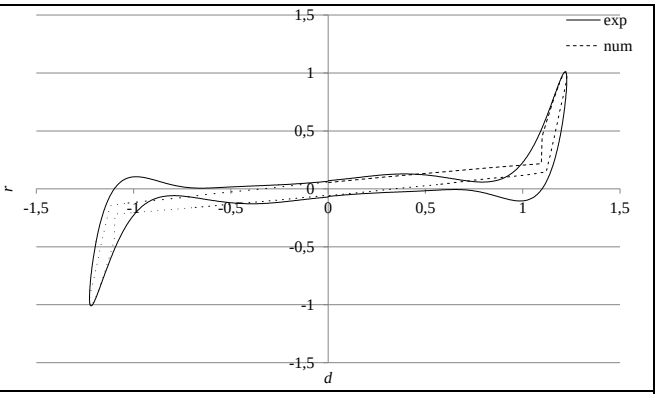


**Fig. 15** YBs, $a_G$=0.05 (solid line: experimental results, dashed line: numerical results) - Inertia force *vs*. relative displacement at resonance

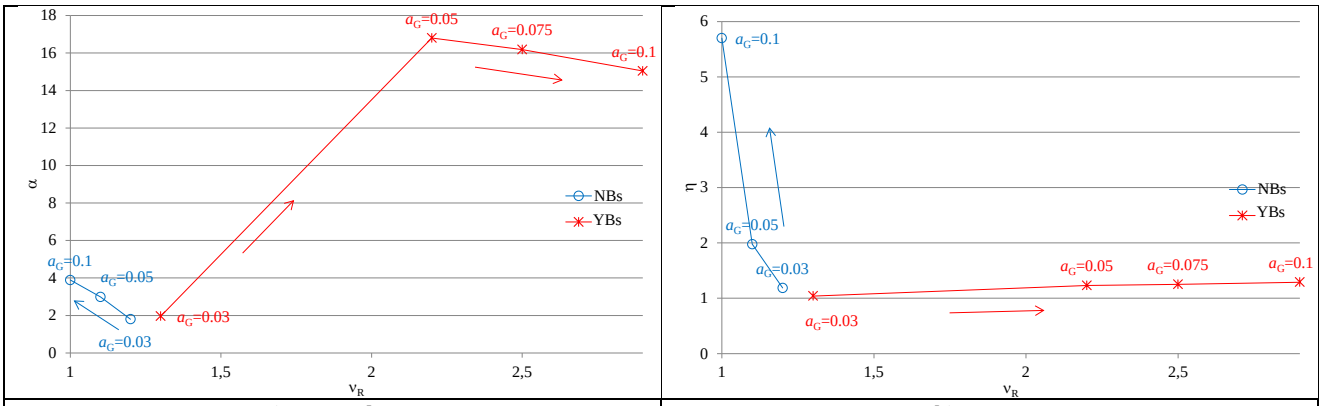


a) Acceleration b) Excursion

**Fig. 16** NBs (blue line with circle indicators) and YBs (red line with star indicators) in terms of excitation frequency

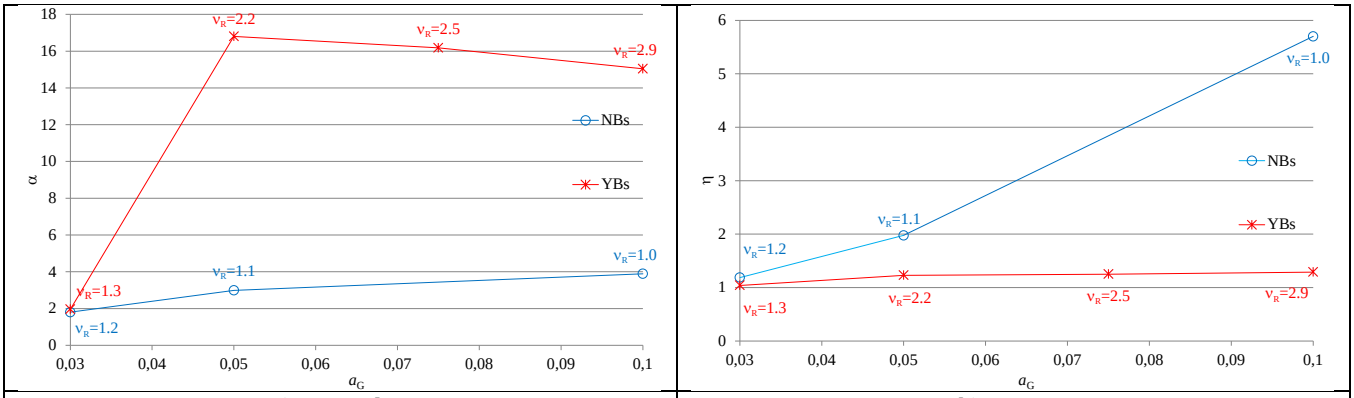


a) Acceleration b) Excursion

**Fig. 17** NBs (blue line with circle indicators) *vs.* YBs (red line with star indicators) in terms of table acceleration

**Table 1** Symbols and acronyms

| | |
|---|---|
| $M$ | mass |
| $K_{ed}$ | damper's elastic stiffness |
| $K_{hd1}$ | damper's 1st hardening stiffness |
| $K_{hd2}$ | damper's 2st hardening stiffness |
| $R_{yd1}$ | damper's 1st yielding force |
| $R_{yd2}$ | damper's 2st yielding force |
| $K_{eb}$ | bumpers' elastic stiffness |
| $C_d$ | damper's damping coefficient |
| $C_b$ | bumpers' damping coefficient |
| $\Delta_R = \Delta_L = \Delta$ | gap's amplitude |
| $D$ | mass relative displacement |
| $D_d \equiv D$ | damper relative displacement |
| $D_b = D - \triangle$ | bumper relative displacement |
| $D_{yd1}$ | damper's 1st yielding displacement |
| $D_{yd2}$ | damper's 2st yielding displacement |
| $R_b$ | current value of damper force |
| $R_b$ | current value of bumper's force |
| $\Delta_{0j}(t)$ | initial gap |
| $\Delta_j(t) = \Delta_{j0}(t) + D_{bj}(t) - D_d(t)$ | gap function |
| $g$ | gravity's acceleration |
| $A$(t) | acceleration time-history of the table |
| $A_t$ | table acceleration peak |
| $a_G = A_t / g$ | nondimensional table acceleration peak |
| $f$ | frequency |
| $\Delta f$ | frequency increment |
| $\Omega$ | circular frequency of sinusoidal table acceleration |
| $\Omega_{min}$ | minimum circular frequency of sinusoidal table acceleration |
| $D_{tmax} = A_t / (\Omega_{min})^2$ | maximum value of the imposed displacement |
| $\nu_R$ | pseudo-resonance frequency |
| $\Delta\nu_C$ | contact frequency range |
| $A_{max}$ | maximum absolute acceleration |
| $\alpha$ | nondimensional maximum absolute acceleration |
| $D$ | relative displacement |
| $D_{max}$ | maximum relative displacement |
| $D_{min}$ | minimum relative displacement |
| $D = \mathrm{D} / \triangle$ | nondimensional relative displacement |
| $E$ | relative excursion |
| $E_{max}$ | maximum relative excursion |
| $\eta = (D_{max} - D_{min}) / \Delta$ | nondimensional relative excursion |
| $e = E / D_{tmax}$ | nondimensional relative excursion without bumpers |
| $F_I$ | force of inertia |
| $R = F_I / (Mg)$ | dimensionless inertia force |
| $\Delta\nu_C$ | contact frequency range |
| $v_i$ | input velocity |
| $v_o$ | output velocity |
| $s$ | coefficient of restitution |
| $I$ | impulse momentum |
| $\Delta t_c$ | contact time |
| $F_m$ | mean contact force |
| $E_d$ | dissipated energy |
| SDOF | Single-Degree-Of-Freedom |
| EPDM | Ethylene-Propylene Diene Monomer |
| Bs | bumpers |
| YBs | system configuration with bumpers |
| NBs | system configuration without bumpers |

**Table 2** Maximum non-dimensional values of accelerations and excursions

| | $a_G$ | 0.03 | | | | 0.05 | | | | 0.075 | | | | 0.1 | | | |
|---|---|---|---|---|---|---|---|---|---|---|---|---|---|---|---|---|---|
| | | | $\nu_R$ | $\alpha$ | $\eta$ | | $\nu_R$ | $\alpha$ | $\eta$ | | $\nu_R$ | $\alpha$ | $\eta$ | | $\nu_R$ | $\alpha$ | $\eta$ |
| NBs | | | 1.2 | 1.8 | 1.03(*) | | 1.1 | 2.99 | 1.72(*) | | | | | | 1.0 | 3.89 | 2.48(*) |
| | $\Delta$[m] | $\Delta\nu_C$ | | | | $\Delta\nu_C$ | | | | $\Delta\nu_C$ | | | | $\Delta\nu_C$ | | | |
| YBs | 0.03 | 1.3 | 1.3 | 1.96 | 1.04 | 0.7-2.3 | 2.2 | 16.80 | 1.23 | 0.7-2.6 | 2.5 | 16.18 | 1.25 | 0.7-3.1 | 2.9 | 15.04 | 1.29 |

(*) The values of $\eta$ NBs are normalized with respect to the maximum value of the applied displacement, $D_{tmax} = A_t / (\Omega_{min})^2$: 0.02073, 0.03455, 0.0691 m, for $a_G$= 0.03, 0.05, 0.1, respectively.

**Table 3** Impact characterization at resonance: contact forces and times

| | $a_G$ | 0.03 | | 0.05 | | 0.075 | | 0.1 | |
|---|---|---|---|---|---|---|---|---|---|
| | | $F_m/mg$ x $10^{-3}$ | $\Delta t_c$ [ms] | $F_m/mg$ x $10^{-3}$ | $\Delta t_c$ [ms] | $F_m/mg$ x $10^{-3}$ | $\Delta t_c$ [ms] | $F_m/mg$ x $10^{-3}$ | $\Delta t_c$ [ms] |
| | $\Delta$[m] | | | | | | | | |
| YBs | 0.03 | $\cong 0$ | 9 | 14 | 15 | 12 | 23 | 7 | 31 |

**Table 4** Impact characterization at resonance: dissipated energies and coefficients of restitution

| | $a_G$ | 0.03 | | 0.05 | | 0.075 | | 0.1 | |
|---|---|---|---|---|---|---|---|---|---|
| | | $E_d/m$ [(m/s)$^2$] x $10^{-4}$ | $s$ | $E_d/m$ [(m/s)$^2$] x $10^{-4}$ | $s$ | $E_d/m$ [(m/s)$^2$] x $10^{-4}$ | $s$ | $E_d/m$ [(m/s)$^2$] x $10^{-4}$ | $s$ |
| | $\Delta$[m] | | | | | | | | |
| B1 | 0.03 | $\cong 0$ | $\cong 1$ | 3.81 | 0.89 | 17.6 | 0.80 | 15.52 | 0.75 |